Academic Journal of Science and Technology
ISSN: 2771-3032 | Vol. 14, No. 3, 2025

Preparation and Properties of $MA_{0.9}FA_{0.1}PbI_3$ Perovskite Solar Cells by Br^- doping

Yunpeng Zhao, Hari Bala*, Fei Cheng, Yingjie Wen, Boji Wang

Henan Polytechnic University, Jiaozuo, China
* Corresponding author

Abstract: In this study, under fixed cation stoichiometry, the effects of Br^- doping with varying ratios on the structural and optoelectronic properties of perovskite films and corresponding device performance were systematically investigated. The substitution of Br^- for partial I^- in the perovskite lattice demonstrated significant morphological refinement and enhanced crystallographic quality, as evidenced by reduced defect density and grain boundary formation. The optimized composition, $MA_{0.9}FA_{0.1}PbI_{2.85}Br_{0.15}$, exhibited superior film uniformity and crystallinity, which translated into improved photovoltaic parameters in carbon-electrode-based perovskite solar cells (PSCs). The champion device achieved a power conversion efficiency (PCE) of 9.33%, outperforming the undoped $MA_{0.9}FA_{0.1}PbI_3$ counterpart. Environmental stability assessments revealed that unencapsulated Br^--doped devices maintained 92% of their initial PCE after 60 days in ambient atmosphere (25°C, 40–60% RH), demonstrating markedly enhanced operational durability compared to the undoped control group. This work highlights halogen engineering as an effective strategy for simultaneously optimizing phase stability and defect passivation in mixed-halide perovskite systems.

Keywords: Perovskite solar cells; $MA_{0.9}FA_{0.1}PbI_{2.85}Br_{0.15}$; Carbon electrode; Stability.

1. Introduction

Organic-inorganic hybrid perovskite materials exhibit significant advantages in optoelectronic applications due to their unique structural configuration and exceptional optoelectronic properties, including: High absorption coefficient and broad spectral response, Long carrier lifetime and high charge carrier mobilitym Tunable bandgapm Solution processability and Flexibility in interface engineering[1, 2]. Organic-inorganic halide perovskite solar cells (PSCs) have developed rapidly, and the proven photoelectric conversion efficiency (PCE) can be comparable to that of silicon-based solar cells. Despite the rapid development of PSCs in recent years, the devices prepared at room temperature have low stability and the surface topography of the devices is not very good. Therefore, it is necessary to find a suitable method to prepare the devices with high quality perovskite films, fewer grain boundaries and high carrier transmission efficiency, so as to obtain high photoelectric conversion efficiency and high environmental stability. The chemical solution method is widely used for perovskite film fabrication due to its ease of operation and low cost, primarily categorized into one-step spin-coating and two-step spin-coating approaches. While the one-step spin-coating method offers simplicity in processing, it suffers from uncontrollable crystallization rates of perovskite, which leads to high carrier recombination rates in perovskite solar cells (PSCs). This ultimately results in the formation of non-uniform and non-compact perovskite films with compromised optoelectronic properties[3-6]. Perovskite solar cell (PSC) devices fabricated via the two-step spin-coating method exhibit enhanced reproducibility, with uniform-quality perovskite thin films achieved through precise control over film thickness and crystal growth kinetics. This methodology significantly improves long-term stability and photoelectric conversion efficiency (PCE) by optimizing morphological homogeneity and suppressing defect states in the perovskite active layer[5, 7-9]. However, element doping can broaden the absorption range of visible light and inhibit the recombination of photogenerated carriers, so as to obtain higher quality perovskite films and obtain higher PCE. Bandar Ali Al-Asbahi's research group used a two-step method to prepare perovskite films. First, a high-concentration PbI_2 solution was formed, and the layered structure of PbI_2 was prepared, which meant that the insertion of MA^+ was easy to achieve. Then, $MAPbI_3$ was generated by reacting with MAI, and the crystallization of perovskite was controlled by two-step method. The film uniformity and perovskite crystallinity are higher than that of one-step method[10]. In addition, it has been found that ion doping can change the surface morphology of perovskite films, and researchers use formamidine ions (FA^+) with a larger radius than MA^+ to improve the thermal stability of the device. However, the stability of pure $FAPbI_3$ is still poor in high humidity environment, and it is easy to decompose into other phases such as PbI_2, and there is no light absorption ability. Recent studies have found that the addition of FA^+ will further reduce the band gap of the light absorption layer, making perovskite materials closer to the theoretical optimal photovoltaic ban[11]. Michael Ng et al. doped Cl^- in $FAPbBr_3$ and found that after doping Cl^-, the surface morphology of perovskite films was improved and showed excellent stability[12]. Thiri Htun et al., by introducing different concentrations of Fe doping into inorganic, lead-free, non-toxic and stable $Cs_3Bi_2Br_9$ perovskite, transformed the original $Cs_3Bi_2Br_9$ with a band gap of 2.54 eV to 1.78 eV after 70% Fe doping, and adjusted the bandgap energy and crystal structure through B-substitution[13]. In order to inhibit the oxidation of B-site ions and improve the structure of PCE, Mg^{2+} and Br^- double doping into $FASnI_3$, Zhang et al obtained $FASn_{0.75}Mg_{0.25}I_2Br$ with high stability and excellent performance. The results of geometric and photoelectrical properties all show that proper doping can increase the stability and adjust the band gap. Improve charge transfer

balance[14].

When a certain amount of Br^- is added to the solution of PbI_2, the radius of Br^- ion is smaller than the radius of I^- ion, the crystallization ability of perovskite films will be enhanced, the grain size and material band gap will be increased, and then the carrier recombination will be inhibited and the contact resistance will be reduced, which is conducive to the extraction and transport of carriers at the interface[15-17]. In addition, in this paper, the proportion of FA^+ doping is kept constant, and Br^- is added to the precursor solution of PbI_2. The incorporation of Br^- will reduce the lattice constant of perovskite, thus making the structure of perovskite stable. Most of the current lab-made perovskite solar cells usually have a precious metal as the top electrode. However, the large-scale use of metal-top electrodes has disadvantages, such as inducing degradation of perovskite, requiring high-temperature deposition under vacuum, and low scalability. The carbon electrode has the advantages of conductivity, flexibility, low cost and easy manufacturing[18-20].

2. Experimental

2.1. Materials and preparation

Dimethyl sulfoxide (DMSO, 99.9%), Titanium tetrachloride ($TiCl_4$, 99%), Diethanolamine (DEA,99.9%), Chlorobenzene(CB,99%), hydrogenperoxide (H_2O2,99%) and Zirconium(ZrO_2, 99.99%) were purchased from Shanghai Macklin Biochemical Co, Ltd Ltd, N-dimethylformamide (DMF, 99.8%) was purchased from Aladdin Reagent Co., LTD. Titania (TiO_2, 99.99%), FAI,PbI_2,MAI and $PbBr_2$were purchased from Xian Polymer Light Technology Corp. Fluorine-doped tin oxide conductive substrates (FTO, ≤7 Ω/sq) were purchased from Shenzhen South China Xiangcheng Technology Co. Ltd. China. The carbon paste (printing ink) was purchased from Jujo Printing Supplies & Technology (Ping hu) Co. Ltd.

2.1.1. Device fabrication

The device is prepared in an air atmosphere with a humidity of 30%-60%. The glass with FTO layer is etched with zinc powder and 5mol/L hydrochloric acid, and the etched glass is cleaned with detergent, deionized water, acetone and ethanol in turn, and then dried in clean air at 100℃. Then a TiO_2 (BL-TiO_2) film ($Ti(OC_4H_9)_4$: DEA: CH_3CH_2OH volume ratio) is rotated at 40000 rpm for 20s. BL-TiO_2 film was dried and annealed at 500℃ for 30 min, the substrate was treated with $TiCl_4$ solution at 70℃, and then washed with distilled water and ethanol respectively. Mesoporous TiO_2 (ML-TiO_2) was prepared by spinning 20s at 3000 rpm. The resulting film is then dried and annealed at 500°C for 30 minutes, cooled to room temperature, and the substrate is treated again with a diluted $TiCl_4$ solution. Then, mesoporous ZrO_2 (ML-ZrO_2) was prepared by spinning 20s at 3000 rpm. The preparation of the perovskite layer is prepared by a two-step method. First, the mixed solution of PbI_2 and $PbBr_2$ is prepared, and the mass required for the preparation of PbI_2 and $PbBr_2$ is calculated according to different molar ratios. The weighed drug is put into the DMF/DMSO mixed solvent (the volume ratio is 9:1). Add 65μL preheated 1.5mol/L PbI_2 and $PbBr_2$ mixed solution onto the substrate prepared in the above steps, spin coating at 1500 r/min for 20 s, spin coating substrate on the heating table at 70 ℃ for 30 min, and then cool to room temperature. The second step was to prepare a mixture of FAI and MAI (the molar ratio of MAI and FAI in IPA was 9:1), preheat the mixture at 40℃, spin coating at 1500 r/min for 30 s, and then annealing the spin-coated substrate at 100℃ for 30min and cooling to room temperature to obtain black perovskite film. After the preparation of the perovskite film, the carbon paste is scraped onto the perovskite film and dried at 100°C for 15 minutes to obtain PSC, with an effective area of 0.1 cm^2.

2.2. Characterization

The surface morphology of perovskites was first observed using scanning electron microscopy (SEM, Carl Zeiss Microimaging GmbH, Germany). Micro - and nano-scale topography observation and in situ spm imaging were performed by the nanomechanical Properties testing System (Hysitron Instruments, Inc.). The scanning imaging rate of SPM imaging was 0.5HZ, the setting force was 2mN, and the scanning size was 10μm. X-ray diffractometer (Rigaku Corporation, Japan) was used to measure the diffraction Angle and intensity to determine the crystal structure, lattice parameters and phase composition of the material. With TU-1810PCS UV-Vis spectrophotometer, the structure of the compound was determined and the properties of the compound were characterized. With glass with FTO as a blank control group, the absorption spectra of perovskite films were determined by spectrophotometer with the range of 400-900 nm. The photoluminescence (PL) spectrum of photoinduced luminescence was then measured using a steady-state fluorescence spectrometer (Edinburgh FLS1000) with a test range of 650-850 nm and an excitation wavelength of 467 nm. Solar simulator BOS-X-1000G was used to test the prepared device, and the irradiance was 100mW/cm2, equivalent to the solar radiation under the spectrum of AM1.5G. keithley2602-A digital power meter was used to apply bias voltage to both ends of the solar cell for scanning, and the current value of its external circuit was measured. The J-V characteristic curve is obtained. Electrochemical workstation (CHI660E B193227, Co., LTD.) was used to measure the electrochemical impedance profile of PSCs in the frequency range of 100MHz-100kMHz with a bias of 0.1V. Then the water resistance of perovskite active layer was studied by using a contact Angle measuring instrument (Dhhv1351UM). The suspension drop method was used to measure the water resistance. The contact Angle measuring range was $0<\theta<180°$.

3. Results and Discussion

3.1. Structures Descriptions

The structure diagram of the prepared device and the working principle of the perovskite solar cell are shown in Figure 1. The device structure is FTO/BL-TiO_2 / ML-TiO_2 / ML-ZrO_2 / perovskite/C, and the perovskite material is filled in the ZrO_2 and TiO_2 mesoporous layers, and covered on the surface of the ZrO_2 layer. When exposed to visible light, photons within the perovskite layer are absorbed and internal electrons are excited to transition from the valence band to the conduction band, creating an electron-hole pair in which electrons and holes migrate to the negative and positive poles, respectively. When the FTO and the carbon electrode are connected through an external circuit, the carriers move in a directional direction due to the potential difference between the two sides, resulting in an electric current.

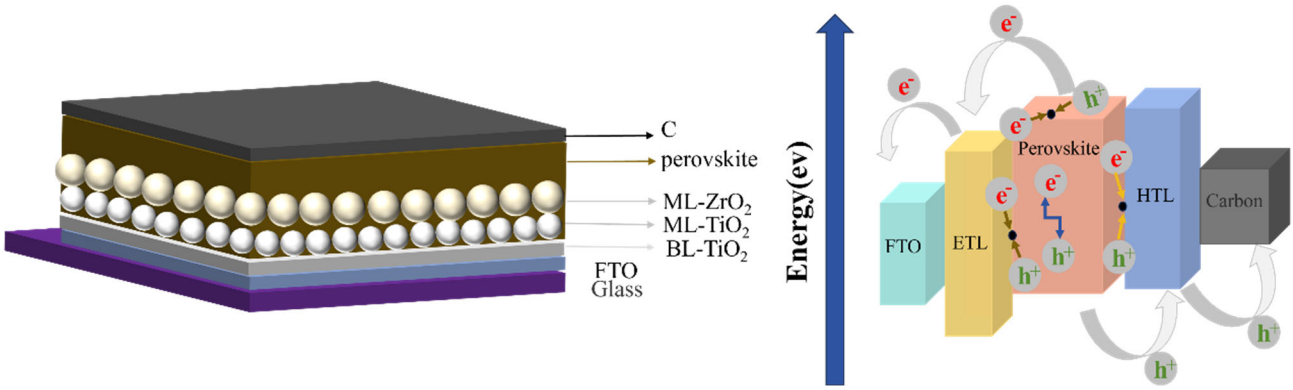

Figure 1. Structure of the device and the working principle of the perovskite solar cell

To explore the effect of Br^- doping on the surface morphology of the prepared devices, $FA_{0.1}MA_{0.9}PbI_3$ perovskite films were prepared on the substrate of FTO/TiO_2 compact layer /TiO_2 mesoporous layer /ZrO_2 mesoporous layer as a control group. After doping different proportions of Br^-, the perovskite films of $MA_{0.9}FA_{0.1}PbI_{2.9}Br_{0.1}$, $MA_{0.9}FA_{0.1}PbI_{2.85}Br_{0.15}$, $MA_{0.9}FA_{0.1}PbI_{2.8}Br_{0.2}$ and $MA_{0.9}FA_{0.1}PbI_{2.7}Br_{0.3}$ were taken as the experimental group. The side morphology of FTO/TiO_2 dense layer /TiO_2 mesoporous layer /ZrO_2 mesoporous layer/perovskite active layer observed by scanning electron microscope is shown in Figure 2:

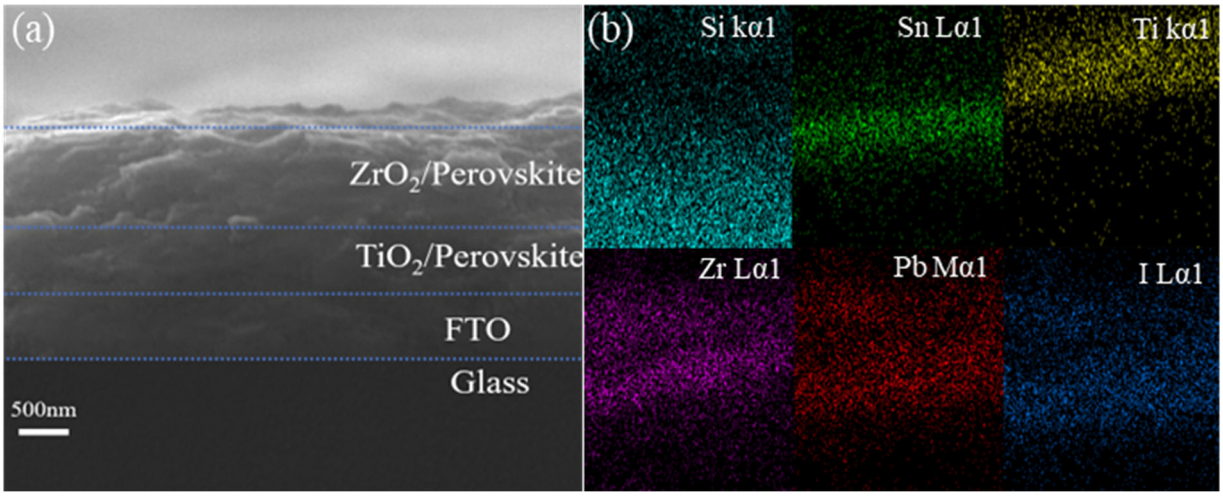

Figure 2. (a) Side SEM images of FTO/TiO_2 compact layer /TiO_2 mesoporous layer /ZrO_2 mesoporous layer/perovskite layer; (b) EDS diagrams of Si, Ti, Sn, Zr, Pb and I elements on thin film cross sections

From Figure (a), it can be seen that the thickness of FTO layer is about 590nm, and the thickness of TiO_2 mesoporous layer and ZrO_2 mesoporous layer is about 500nm. Perovskite grows in the mesoporous layer, and filling the mesoporous layer with perovskite particles will make the surface film quality of perovskite smoother, and the carrier will be better transported, increasing its transport channel. In turn, the efficiency of photoelectric conversion becomes higher. The corresponding distribution diagram of each element in the device is shown in Figure (b), and the distribution of elements in Figure (b) corresponds well to that in Figure (a). Si exists in conductive glass, Sn, Ti and Zr reflect the existence position of FTO layer, TiO_2 dense layer, TiO_2 mesoporous layer and ZrO_2 mesoporous layer, and Pb and I are components of perovskite. Perovskite particles grow in the mesoporous layer, which again corresponds well to figure (a). As can be seen from Figure 2, the thickness of perovskite filling in the TiO_2 mesoporous layer and ZrO_2 mesoporous layer is about 800nm, and continues to extend upward to about 1000nm on the surface. This structure allows perovskite particles to grow and crystallize in the mesoporous layer, which can control the crystal size of perovskite and allow perovskite to crystallize well.

3.2. Surface topography analysis

In Figure 3, they are (a)$MA_{0.9}FA_{0.1}PbI_3$, (b)$MA_{0.9}FA_{0.1}PbI_{2.9}Br_{0.1}$, (c)$MA_{0.9}FA_{0.1}PbI_{2.85}Br_{0.15}$, (d)$MA_{0.9}FA0.1PbI_{2.8}Br_{0.2}$ and (e)$MA_{0.9}FA_{0.1}PbI_{2.7}Br_{0.3}$ SEM and SPM images of the surface of perovskite film show that perovskite crystals grow irregularly on the mesoporous layer, and the crystals are scattered and stacked, not densely arranged, and the surface is rough. After doping Br^- in (b), the perovskite crystals show irregular shape, there are connections between crystals, irregular holes in the middle, more grain boundaries on the surface, and the whole is not smooth. With the increase of Br^- concentration, the surface of the perovskite film becomes smooth, the surface roughness is smaller, the internal defects are reduced, the grain boundaries are reduced, and the quality of the film is improved as shown in figure c1 and c2. It can be seen from Figure (d) that although the surface morphology of perovskite has been improved, there are still more surface defects, and the grain boundaries have increased and the film quality has decreased compared with Figure (c). In Figure (e), the crystals are arranged loosely and irregularly, some of which appear as bladed crystals, interspersed in the perovskite film, with many

defects, which is not conducive to carrier transmission. Excessive doping of Br^- cannot improve the surface topography, but will reduce the quality of the surface film. Therefore, $MA_{0.9}FA_{0.1}PbI_{2.85}Br_{0.15}$ has better film quality, and the crystal quality on the film surface is the best.

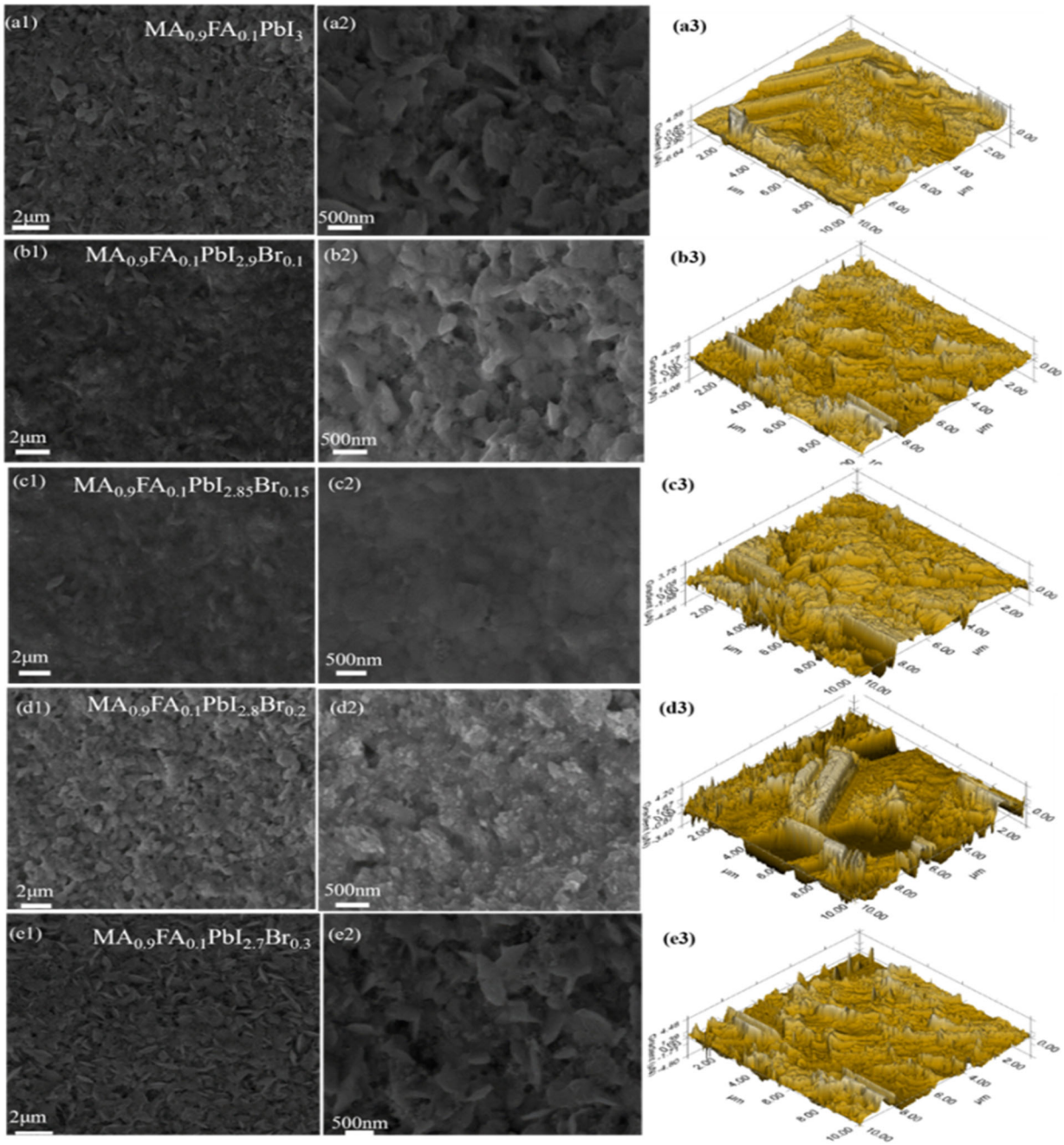

Figure 3. (a) $MA_{0.9}FA_{0.1}PbI_3$, (b) $MA_{0.9}FA_{0.1}PbI_{2.9}Br_{0.1}$, (c) $MA_{0.9}FA_{0.1}PbI_{2.85}Br_{0.15}$, (d) $MA_{0.9}FA_{0.1}PbI_{2.8}Br_{0.2}$, (e) SEM and SPM images of the surface of $MA_{0.9}FA_{0.1}PbI_{2.7}Br_{0.3}$ film

3.3. Crystal Structure and Properties Descriptions

The effect of Br^- doped concentration on the phase purity and crystallization properties of perovskite films can be studied by XRD analysis. As shown in Figure 4, after Br^- doping, no new diffraction peaks appeared and no other hybrid peaks were introduced, and Br^- doping did not cause the transformation of perovskite crystal type. At 2θ of 13.5°, 27.8° and 31.4°, the diffraction peaks of (110), (220) and (312) perovskite crystal plane are corresponding, respectively. It can be seen from Figure 4 that the diffraction peak of doped perovskite thin film does not change significantly compared with that of undoped thin film. However, with the increase of doping concentration, the peak shape of $MA_{0.9}FA_{0.1}PbI_{2.85}Br_{0.15}$ film becomes sharper at 27.8°, and the characteristic peak is enhanced, indicating that the crystallinity of the device is improved, the crystal quality is improved, and there is no lattice distortion. The above results show that the quality of $MA_{0.9}FA_{0.1}PbI_{2.85}Br_{0.15}$ film is the best, which is consistent with the analysis of surface morphology. To further verify this conclusion, we performed other characterization tests on perovskite films with different BR-doping concentrations.

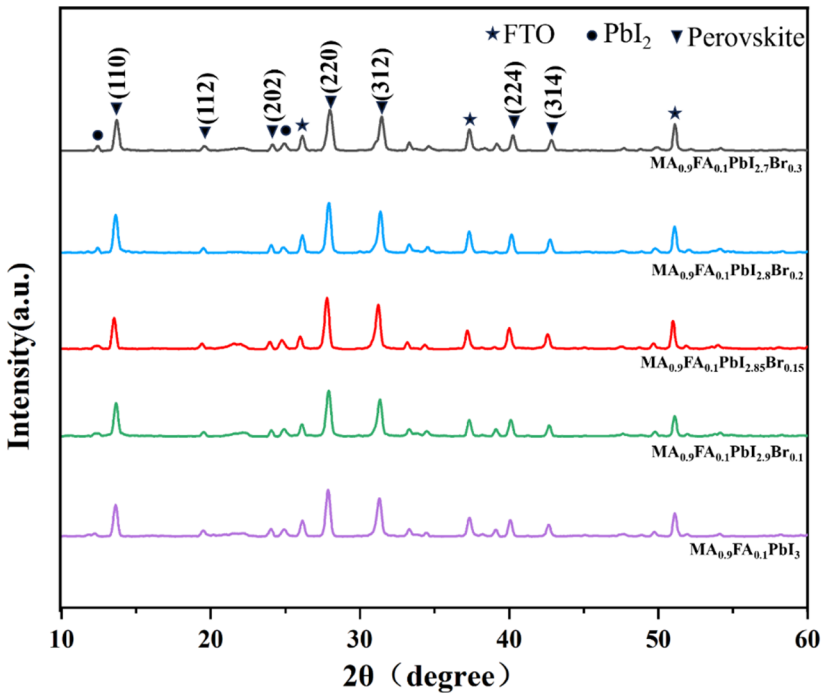

Figure 4. XRD patterns of perovskite doped films with different ratios of Br^-

3.4. Optical Performance Descriptions

The perovskite film on the same substrate was analyzed by UV-Vis absorption spectrum, and the test results are shown in Figure 5. Because the substrate below perovskite has very weak absorption of ultraviolet light, it basically does not affect the test results of perovskite films. At about 800nm, the absorption intensity of the perovskite film to ultraviolet light has a very violent increase. The absorption edge of the control group with undoped Br^- perovskite film is about 750nm, while the absorption edge of the perovskite film with added Br- moves slightly to the direction of low wavelength, which is considered to be the increase of the transition energy level between molecular orbitals caused by doping. According to the formula $\Delta E = hc/\lambda$, when the energy difference increases, the corresponding absorption wavelength λ will decrease, the band gap width of the perovskite doped with Br^- will decrease, and the absorption range will increase. As can be seen from Figure 5, the slope of the light absorption edge of $MA_{0.9}FA_{0.1}PbI_{2.85}Br_{0.15}$ is the largest and the light absorption intensity is significantly higher than that of other perovskite films, indicating that after doping with Br^-, compared with undoped perovskite films, its quality is better, its light absorption rate is improved, and its light capturing ability is higher than that of other samples. Compared with other doped films, $MA_{0.9}FA_{0.1}PbI_{2.85}Br_{0.15}$ films have fewer surface defects and higher film quality, so the films have better optical properties.

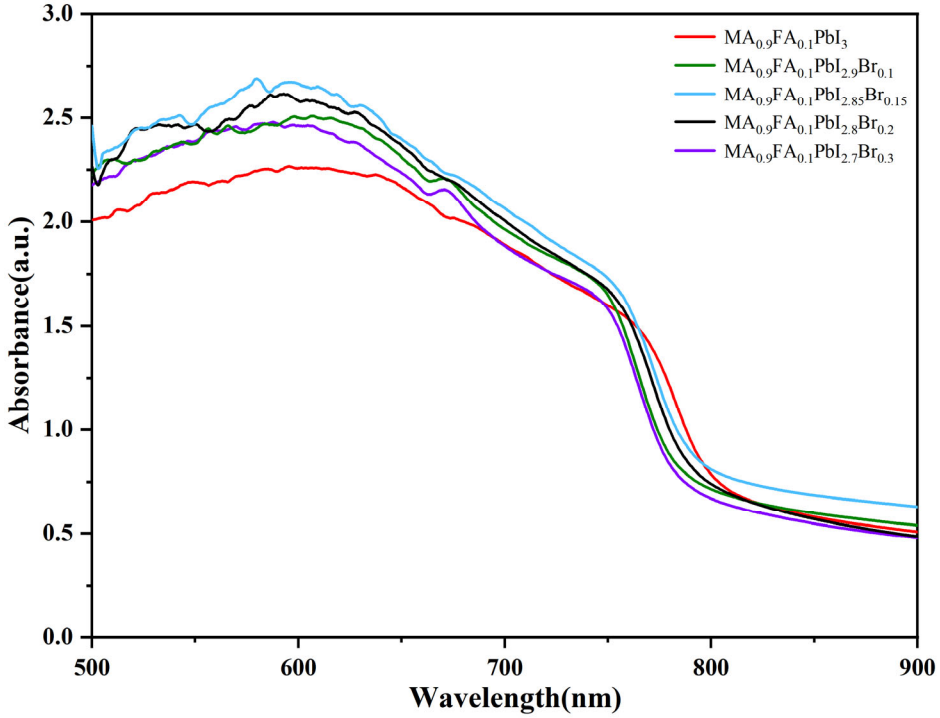

Figure 5. Surface absorption spectra of doped perovskites with different ratios of Br^-

The combination of electrons and holes generated by photoexcitation of perovskite thin films can be understood from the steady-state photoluminescence spectra. PL spectra of doped perovskite thin films with different ratios of Br^- are shown in Figure 6. The peak photoluminescence intensity of perovskite films all appeared at about 780 nm, corresponding to the absorption spectrum results in Figure 5. The steady-state PL spectrum of $MA_{0.9}FA_{0.1}PbI_{2.85}Br_{0.15}$ films showed the weakest intensity, indicating that there was a small degree of non-radiative recombination in the interior of the films, and the surface defects of perovskite films were reduced. Non-radiative electron-hole recombination caused by surface defects is reduced. Therefore, the weaker the PL strength, the less defects inside the device and the less non-radioactive recombination caused by defects. It can be concluded from the above figure that the charge defect at the interface of $MA_{0.9}FA_{0.1}PbI_{2.85}Br_{0.15}$ film is the least, and the film has higher quality. High quality perovskite film is conducive to carrier transport on the surface of perovskite film, which will have higher photoelectric conversion efficiency.

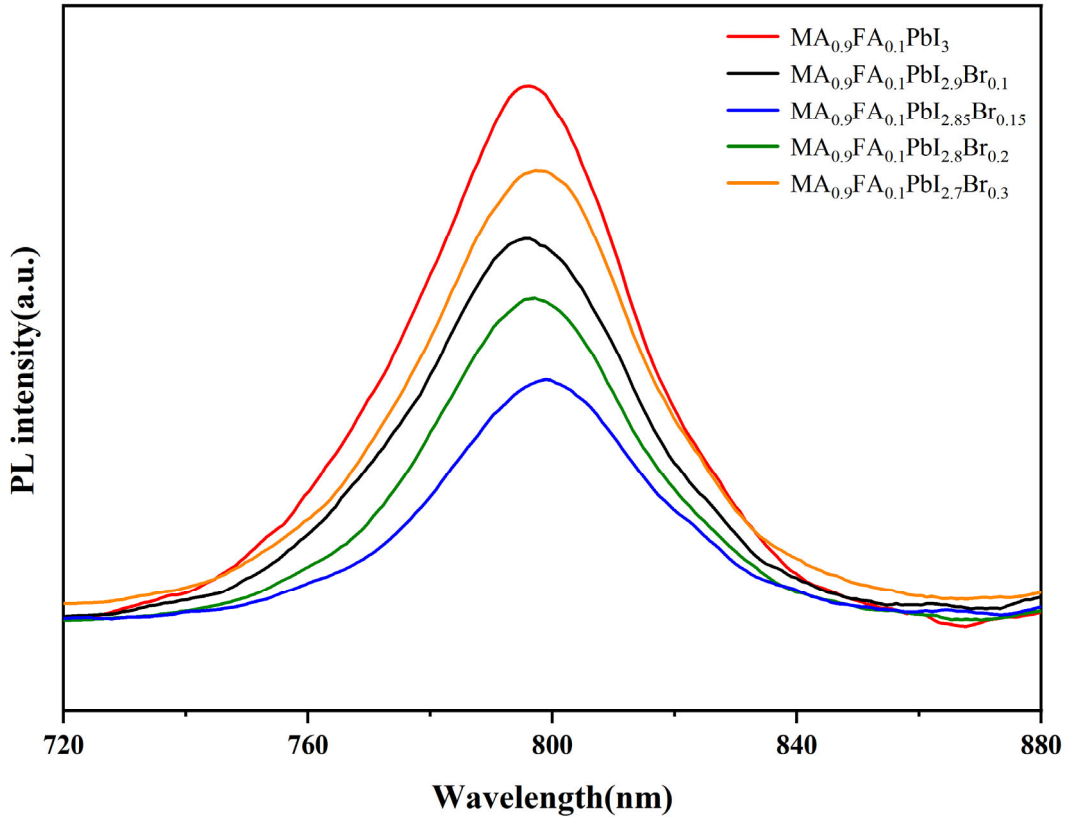

Figure 6. Steady-state emission fluorescence spectra of perovskite doped films with different ratios of Br^-

3.5. Photoelectric Conversion Performance

In order to investigate the effect of different Br^-doping ratio on the photoelectric conversion efficiency and photovoltaic performance of perovskite solar cell devices, simulated sunlight (AM 1.5G, 100 $mW \cdot cm^{-2}$) was used as the light source. A series of carbon-electrode devices were prepared, and the test results obtained were shown in the figure below. All the photovoltaic performance parameters of PSCs prepared by Br^-doping were improved compared with those of undoped PSCs. Voc, *Jsc* and FF of $MA_{0.9}FA_{0.1}PbI_3$-based PSCs were 885mv, 18.32$mA \cdot cm^{-2}$ and 0.48, and PCE was 7.75%, respectively. With the increase of Br^- concentration, when the perovskite film is $MA_{0.9}FA_{0.1}PbI_{2.9}Br_{0.1}$, compared with the undoped device, the Voc and Jsc of the device are increased, which is because the doping of Br^- leads to the improvement of the quality of perovskite film, the reduction of grain boundaries, and better carrier transport. With the increase of Br^-concentration, when the perovskite film is $MA_{0.9}FA_{0.1}PbI_{2.7}Br_{0.3}$, although its voltage is very large, the J_{SC} decreases compared with $MA_{0.9}FA_{0.1}PbI_{2.85}Br_{0.15}$ and $MA_{0.9}FA_{0.1}PbI_{2.8}Br_{0.2}$, and the PCE also decreases. Therefore, in summary, when the perovskite film is $MA_{0.9}FA_{0.1}PbI_{2.85}Br_{0.15}$, its photovoltaic performance parameters in all aspects are relatively good, Voc, *Jsc* and FF are 900mV, 21.18 $mA \cdot cm^{-2}$ and 0.49, and PCE is 9.33%. This is mainly due to the improved film quality of $MA_{0.9}FA_{0.1}PbI_{2.85}Br_{0.15}$, reduced surface defects, improved crystal coverage, and greatly improved light absorption, so the photovoltaic performance of the device has been significantly improved. However, with the continuous increase of Br^- concentration, the photovoltaic performance parameters have not been well improved, because the quality of perovskite films has not continued to increase, the grain boundary between the grains has increased, and the defects have increased.

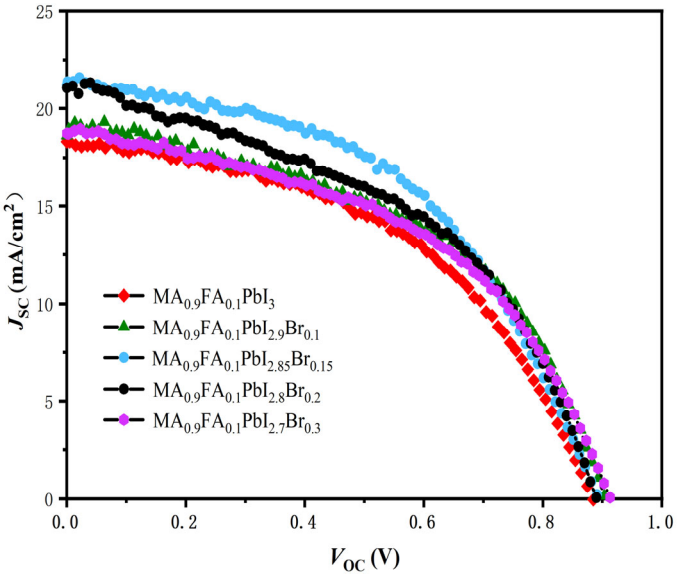

Figure 7. J-V characteristic curves of PSCs with different doping ratios of Br^-

perovskite	V_{OC} (mV)	J_{SC}(mA·cm^{-2})	FF	*PCE* (%)
$MA_{0.9}FA_{0.1}PbI_3$	885	18.32	0.48	7.75
$MA_{0.9}FA_{0.1}PbI_{2.9}Br_{0.1}$	903	18.64	0.51	8.53
$MA_{0.9}FA_{0.1}PbI_{2.85}Br_{0.15}$	900	21.18	0.49	9.33
$MA_{0.9}FA_{0.1}PbI_{2.8}Br_{0.2}$	889	21.01	0.48	8.96
$MA_{0.9}FA_{0.1}PbI_{2.7}Br_{0.3}$	912	18.74	0.48	8.13

3.6. Electrochemical Analysis of Device Internals

In the range of bias voltage of 0.1V and frequency of 10^{-1}Hz to 10^5Hz, electrochemical impedance tests were conducted on PSCs prepared at different Br^- doping concentrations by electrochemical workstation. Figure 8 shows the corresponding equivalent circuit model diagram of solar cells. In the figure, the starting point of the impedance spectrum semicircle corresponds to the series resistance (R_s). Since the prepared PSCs have the same structure, they have similar R_s values, so the starting point of the semicircle is basically the same. The size of the semicircle is proportional to the equivalent composite resistance (R_{rce}) in the device, and the larger the radius of the semicircle, the larger the composite resistance will be. The larger the recombination resistance, the fewer the carrier recombination sites, and the more difficult the recombination of electrons and holes. It can be seen from Figure 8 that the R_{rce} of the Br^-doped device is larger than that of the device composed of undoped films. With the increase of doping concentration, the semicircle becomes larger and the composite resistance becomes larger, but when the film becomes $MA_{0.9}FA_{0.1}PbI_{2.7}Br_{0.3}$, the composite resistance becomes smaller than before. Therefore, it can be concluded that the device composed of $MA_{0.9}FA_{0.1}PbI_{2.85}Br_{0.15}$ thin film has the highest composite resistance, and the interface defects on the surface of the perovskite thin film are reduced, and the crystallization performance is improved, and fewer defects will provide more channels for carrier transmission.

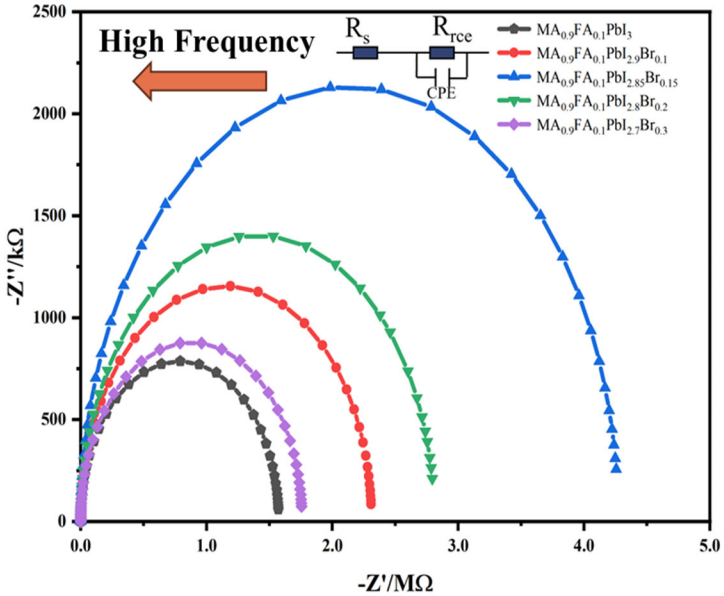

Figure 8. Electrochemical impedance spectra of PSCs doped with different ratios of Br^-

3.7. Stability Analysis

The stability of perovskite cells in the environment is particularly important, and we know that perovskite will decompose when exposed to water in the air for a long time. FIG.9 is the image of $MA_{0.9}FA_{0.1}PbI_3$ and Br^-doped $MA_{0.9}FA_{0.1}PbI_{2.85}Br_{0.15}$ films in direct contact with water, and the contact Angle changes with time within 5min. It can be observed that the contact Angle of the doped film is greater than that of the undoped film within 1-5min. When water was in contact with $MA_{0.9}FA_{0.1}PbI_3$ film at the beginning, the contact Angle was 73.70°, which changed to 60.70° after 1min. However, as the perovskite film reacted with part of the water after a long time of contact with water, the contact Angle decreased to 45.31° when the contact time was 5min. At the beginning of contact between water and $MA_{0.9}FA_{0.1}PbI_{2.85}Br_{0.15}$ film, the contact Angle is 84.37°, which is greater than the initial contact Angle of $MA_{0.9}FA_{0.1}PbI_3$ film, and becomes 62.22° after 1 minute. With the change of time, the contact Angle begins to decrease, reaching 50.34° at 5min. It is also greater than the final contact Angle of $MA_{0.9}FA_{0.1}PbI_3$ film. After Br^- doping, the quality of perovskite is improved, the surface defects are reduced, and the surface moisture resistance is increased.

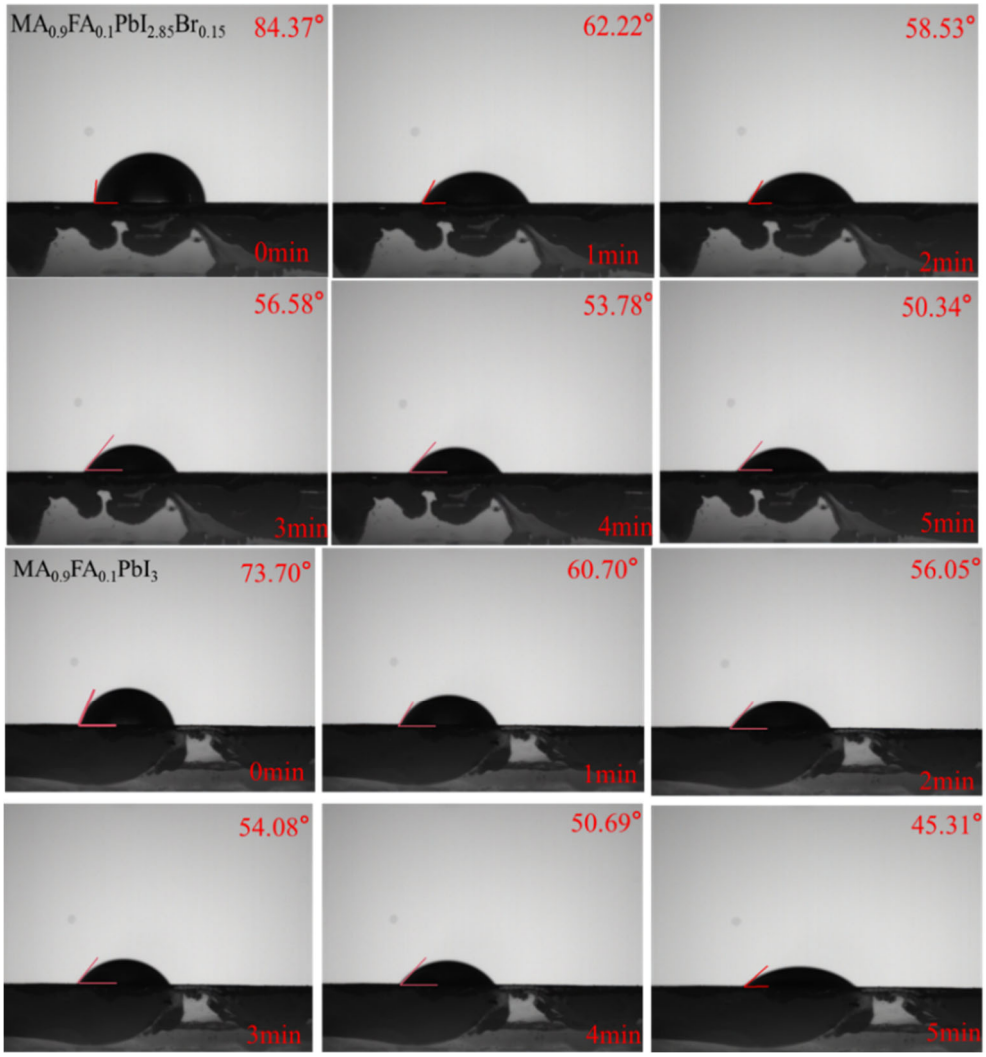

Figure 9. Contact Angle variations between the surface of $MA_{0.9}FA_{0.1}PbI_3$ and $MA_{0.9}FA_{0.1}PbI_{2.85}Br_{0.15}$ films and water at 0, 1, 2, 3, 4 and 5 min

The long-term stability of perovskite solar cells has a very important impact on the future large-scale application and development of solar cells. Therefore, we tested the performance of PSCs prepared with $MA_{0.9}FA_{0.1}PbI_{2.85}Br_{0.15}$ thin films for 60 days in an air atmosphere during the entire fabrication process. The continuous change of its performance parameters in 60 days is shown in Figure 10. As can be seen from the figure, the V_{oc} of the device has remained relatively stable. FF declined in the first few days, and then also stabilized. Compared with the previous J_{sc}, it is considered that with the increase of time, a small part of the surface perovskite crystals encounter water in the air and are exposed to the air environment for a long time and the decomposition occurs, thus affecting the overall performance of the device, resulting in a decline in the overall efficiency. After 60 days, the *PCE* of the device still remains at 92% of the initial *PCE*, indicating that the PSCs prepared by $MA_{0.9}FA_{0.1}PbI_{2.85}Br_{0.15}$ films can still maintain good photoelectric parameters and have good stability after a certain period of time.

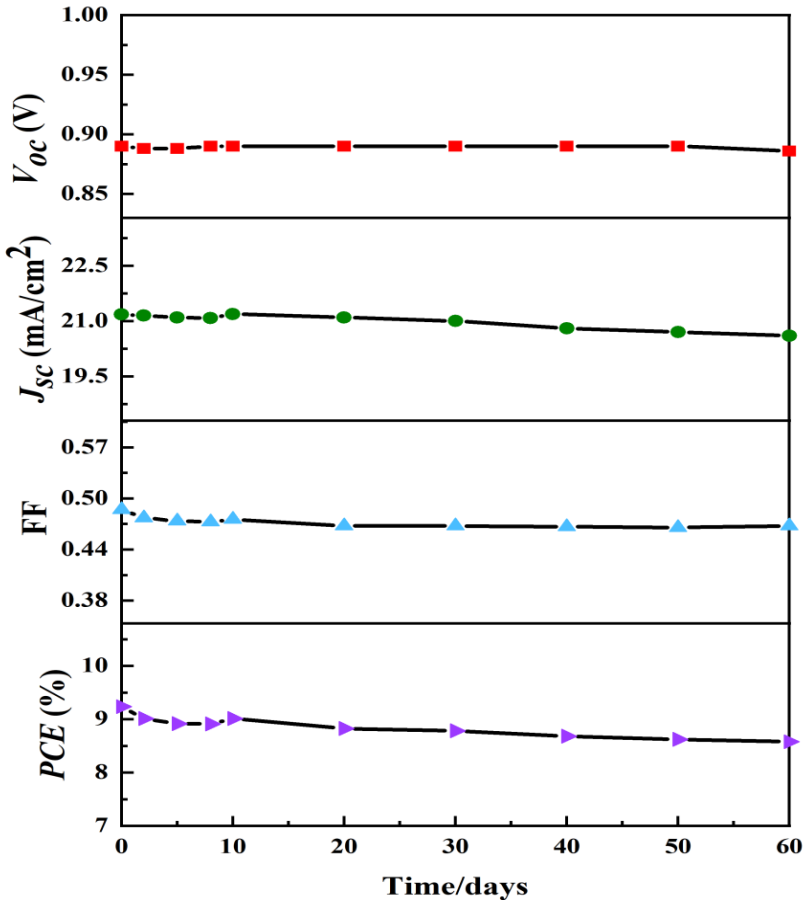

Figure 10. The change curve of the photoelectric parameters of the optimal device after 60 days in an air atmosphere

4. Conclusions

Structure was prepared in air environment atmosphere for FTO/TiO_2 dense layer/ TiO_2 mesoporous ZrO_2/ mesoporous layer/$MA_{0.9}FA_{0.1}PbI_{2.85}Br_{0.15}$/ carbon electrode of perovskite solar cells. The influence of Br^-doping on perovskite films and device properties under the condition of constant FA^+ concentration was investigated, and the best Br^-doping concentration was obtained. Doping changes optimize the surface morphology of the perovskite film, Br^- replaces part of I^-, has a wider light absorption range, reduces the surface defects of the perovskite film, and enhances the stability of the perovskite structure. The doped Br^- concentration in this paper can improve the crystallinity, the quality of the film and the stability of the device. Different concentrations have different effects on the overall photoelectric performance of the device. The effects of different Br^- doping concentrations on the overall performance of the device are compared. Conclusion $MA_{0.9}FA_{0.1}PbI_{2.85}Br_{0.15}$ film has the best surface morphology, increased crystallinity, the best long-term stability, the best film quality and optical properties, and the highest *PCE* of the device is 9.33%. After doping with Br^-, the stability of the device is enhanced and the decomposition rate of perovskite crystals is slowed down. Stored in the air atmosphere for 60 days, its efficiency can still maintain 92% of the initial efficiency, reducing the surface defects of the perovskite film, and ultimately improving its crystallization properties and enhancing the quality of the perovskite film.

References

[1] LIU K, JIANG Y, JIANG Y, et al. Chemical Formation and Multiple Applications of Organic–Inorganic Hybrid Perovskite Materials [J]. Journal of the American Chemical Society, 2018.

[2] ZHANG A, LV Q. Organic-Inorganic Hybrid Perovskite Nanomaterials: Synthesis and Application [J]. ChemistrySelect, 2020.

[3] LI M, XIE Y-M, XU X, et al. Comparison of processing windows and electronic properties between CH3NH3PbI3 perovskite fabricated by one-step and two-step solution processes [J]. Organic Electronics, 2018.

[4] LIU J, WANG M, CAI W, et al. Root cause for the difference in photovoltaic parameters of perovskite solar cells prepared by one- and two-step processes [J]. Applied Physics Letters, 2022.

[5] WANG M, FENG Y, BIAN J, et al. A comparative study of one-step and two-step approaches for MAPbI3 perovskite layer and its influence on the performance of mesoscopic perovskite solar cell [J]. Chemical Physics Letters, 2017.

[6] ZADEH N J, ZARANDI M B, NATEGHI M R. Optical properties of the perovskite films deposited on meso-porous TiO2 by one step and hot casting techniques [J]. Thin Solid Films, 2019.

[7] HAN Y, XIE H, LIM E L, et al. Review of Two-Step Method for Lead Halide Perovskite Solar Cells [J]. Solar RRL, 2022.

[8] WANG C, HE B, FU M, et al. Influence of MACl on the Crystallization Kinetics of Perovskite via a Two-Step Method [J]. Crystals, 2024.

[9] WANG F, GE C, ZHOU X, et al. Manipulation of Crystallization Kinetics for Perovskite Photovoltaics Prepared Using Two-Step Method [J]. Crystals, 2022.

[10] BANDAR ALI A-A. Tuning Photophysical Properties of ZnO/TiO2 Nanocomposite Thin Films by Controlling Anatase Titania Content [J]. ECS Journal of Solid State Science and Technology, 2022.

[11] DENG W, LI F, LI J, et al. Anti-solvent Free Fabrication of FA-Based Perovskite at Low Temperature towards to High

Performance Flexible Perovskite Solar Cells [J]. Nano Energy, 2020.

[12] NG M, HALPERT J E. Single crystals of mixed Br/Cl and Sn-doped formamidinium lead halide perovskites via inverse temperature crystallization [J]. RSC Advances, 2020.

[13] HTUN T, ELATTAR A, ELBOHY H, et al. Lead-free iron-doped Cs3Bi2Br9 perovskite with tunable properties [J]. RSC Advances, 2024.

[14] ZHANG N, LI Y, ZHOU Y, et al. Tuning the Photoelectric Properties of Perovskite Materials Using Mg/Ge/Si and Br Double-Doped to FASnI3 [J]. The Journal of Physical Chemistry C, 2023.

[15] WANG C, CHESMAN A S R, YIN W, et al. Facile purification of CsPbX3(X =Cl−,Br−,I−) perovskite nanocrystals [J]. The Journal of Chemical Physics, 2019.

[16] SELIVANOV N I, MURZIN A O, YUDIN V I, et al. Counterdiffusion-in-gel growth of high optical and crystal quality MAPbX3 (MA = CH3NH3+, X = I−, Br−) lead-halide perovskite single crystals [J]. CrystEngComm, 2022.

[17] XIE Y-M, ZENG Z, XU X, et al. FA-Assistant Iodide Coordination in Organic-Inorganic Wide-Bandgap Perovskite with Mixed Halides [J]. Small, 2020.

[18] BIDIKOUDI M, SIMAL C, STATHATOS E. Low-Toxicity Perovskite Applications in Carbon Electrode Perovskite Solar Cells—A Review [J]. Electronics, 2021.

[19] PRADID P, SANGLEE K, THONGPRONG N, et al. Carbon Electrodes in Perovskite Photovoltaics [J]. Materials, 2021.

[20] WU Z, LIU Z, HU Z, et al. Highly Efficient and Stable Perovskite Solar Cells via Modification of Energy Levels at the Perovskite/Carbon Electrode Interface [J]. Advanced Materials, 2019.